Spatiotemporal Regulation and Functional Divergence of Bmp2 and Bmp7 in Periodontal Injury Response

Yu Fu [a, b, c, d], Daniela M. Roth [c, e], Maria Alexiou [a, b, c], Daniel Graf [a, b, c*]

[a] Department of Oral Biological & Medical Sciences, Faculty of Dentistry, The University of British Columbia, Vancouver, BC, V6T 1Z3, Canada yfu47@student.ubc.ca
[b] Life Sciences Institute, The University of British Columbia, Vancouver, BC, V6T 1Z3, Canada
[c] School of Dentistry, Faculty of Medicine & Dentistry, University of Alberta, Edmonton, AB, T6G 1Z1, Canada
[d] Institute of Stomatology, School and Hospital of Stomatology, Wenzhou Medical University, Wenzhou, 325027, China
[e] Cancer Early Detection Advanced Research Center (CEDAR), Knight Cancer Institute, Oregon Health and Science University, Portland, OR, 97201, USA

*Corresponding author at: Department of Oral Biological and Medical Sciences, Faculty of Dentistry, The University of British Columbia, 2350 Health Sciences Mall Vancouver, BC V6T 1Z3, Canada.
E-mail address: daniel.graf@ubc.ca

Supplementary Figures and Figure legends

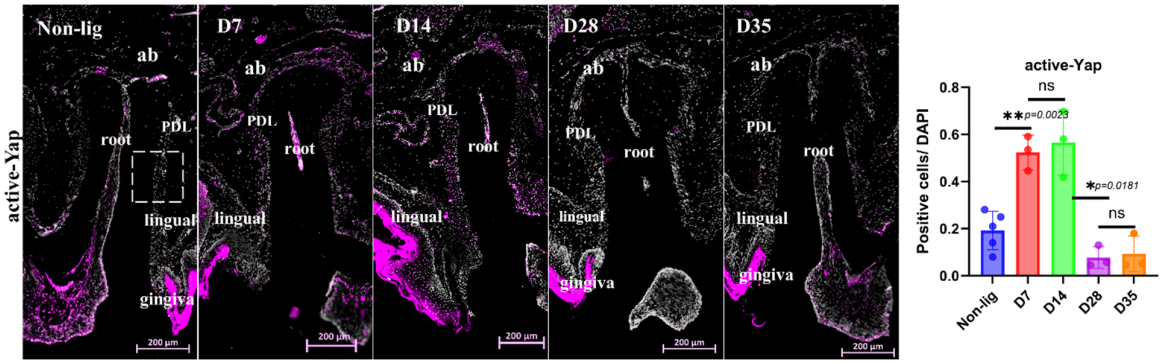

Supplementary Figure 1. Assessed mechanical stimulation using active Yes-associated protein (active-Yap).

Active Yap is broadly distributed throughout the PDL along the tooth length on ligature teeth at days 7 and 14, with minimal signal in non-ligature controls. Scale bar: 200 µm. Quantification confirmed increased active Yap detection.

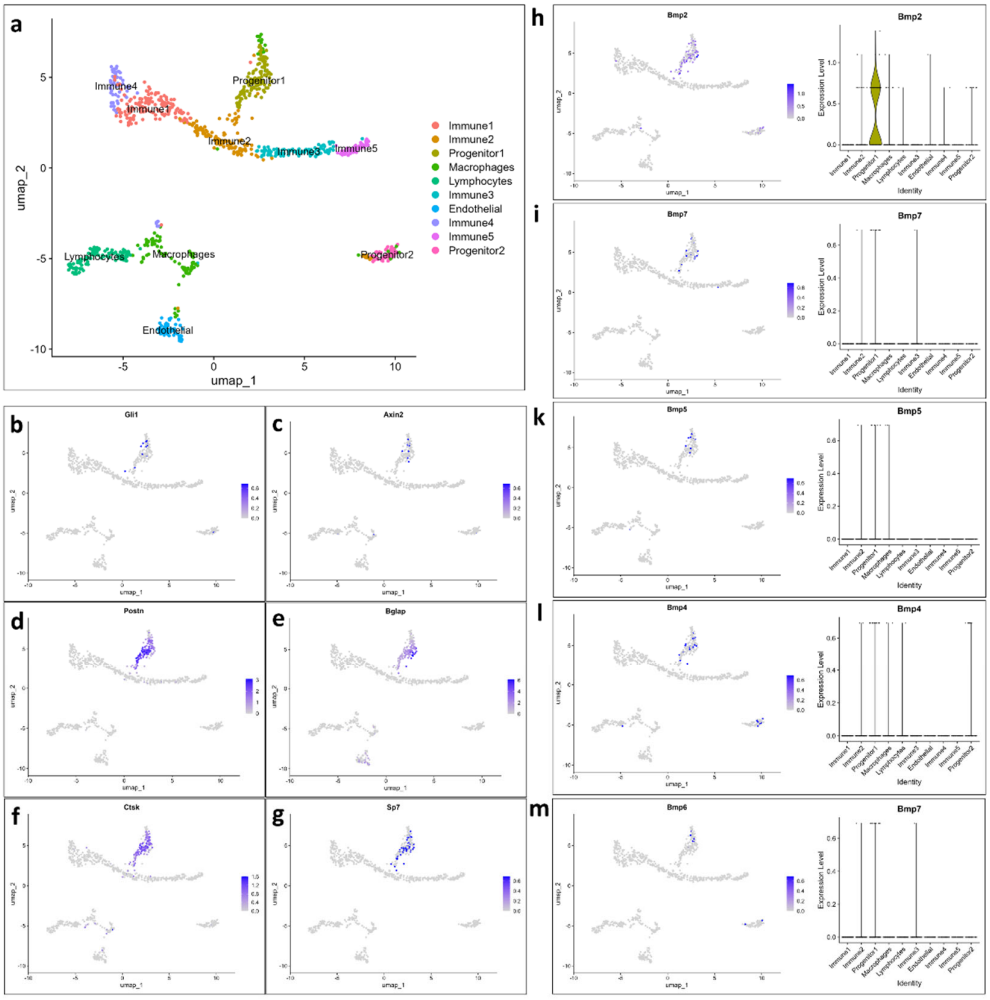

Supplementary Figure 2. scRNA-seq analysis identifies progenitor cells as the primary source of Bmps (Bmp2, 4, 5, 6, 7) in the adult periodontium.

(a) UMAP plot of published scRNA-seq data from adult mouse molar periodontal ligament, showing three major cell types: progenitor, endothelial, and immune cells. **(b-c)** Feature plots of Gli1 and Axin2, marking populations associated with Hedgehog and Wnt signaling pathways **(d)** Feature plots of Postn, highlighting periodontal ligament fibroblasts involved in extracellular matrix organization and tissue remodeling. **(e-g)** Feature plots of Bglap, Sp7, and Ctsk, representing osteogenic and bone remodeling lineages, including mature osteoblasts (Bgalp), osteoprogeniteors (Sp7) and osteoclasts (Ctsk). **(h-m)** Feature plots and violin plots of osteogenic Bmps, showing that Bmp2 is more highly expressed in periodontal ligament cells, suggesting a dominant role in osteogenic signaling and tissue homeostasis. Data can be found at GEO; Access number: GSE160358.

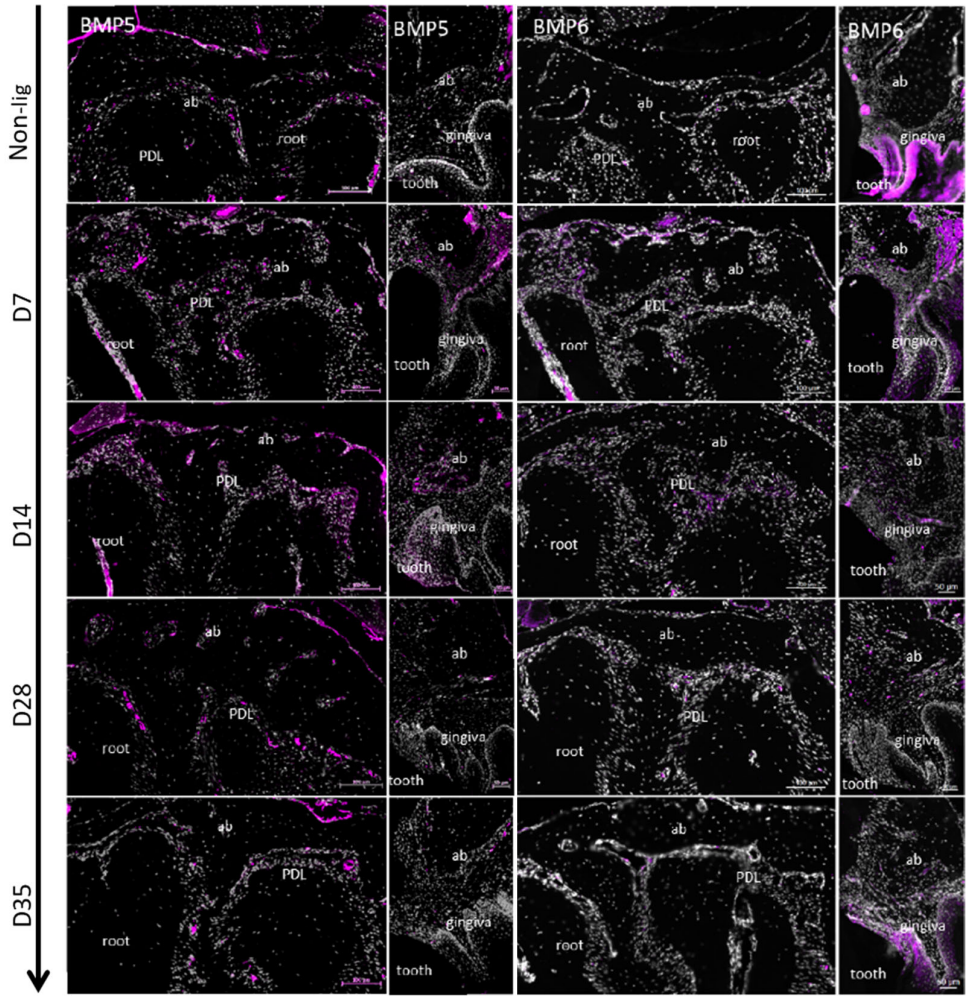

Supplementary Figure 3. Temporal dynamics of BMP 5 & Bmp6 expression in periodontal remodeling.

Immunofluorescence staining of Bmp5 (left) and Bmp6 (right) in ligature-induced mice. Timeline: non-ligated control; days 7 and 14 post-ligature placement; and days 28 and 35 following ligature removal (day 21). Regions of interest: root apical area (scale bar = 100 μm) and alveolar bone crest area (scale bar = 50 μm).

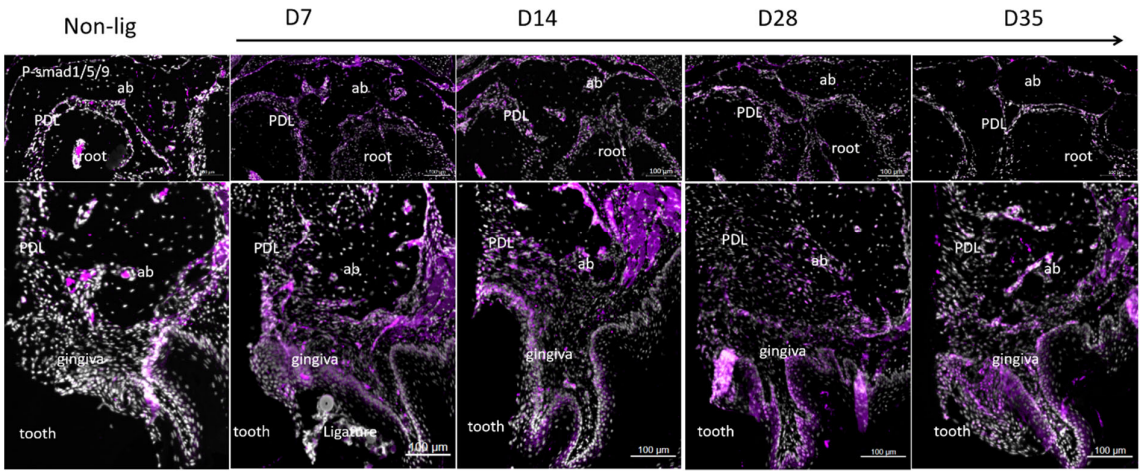

Supplementary Figure 4. Spatial and temporal distribution of p-Smad1/5/9 during ligature-induced periodontal remodeling.

Representative immunofluorescence staining of phosphorylated Smad1/5/9 (p-Smad1/5/9) in frontal sections of the root apical periodontal ligament (PDL) and alveolar bone crest (ABC) on the non-ligature side at Days 7, 14, 28, and 35. Widespread p-Smad1/5/9 expression was observed throughout the PDL at both anatomical sites on Days 7, 14, and 28 which decreased by and 35. Nuclei are counterstained with DAPI. Scale bar = 100 µm.

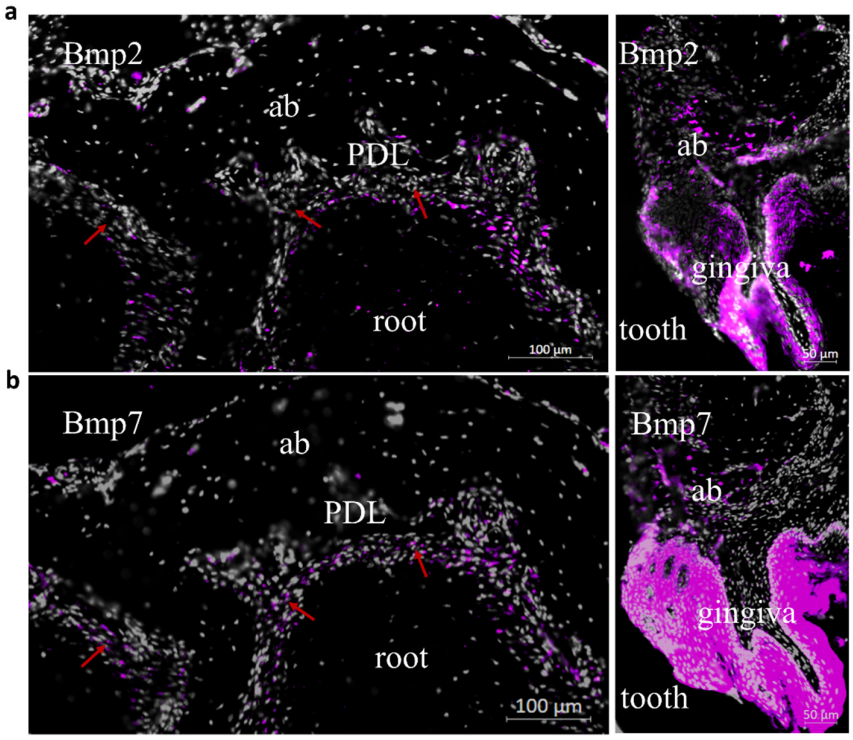

Supplementary Figure 5. Spatial distribution of Bmp2 and Bmp7 ligature-induced periodontal remodeling.

(a) Representative immunofluorescence staining of Bmp2 in frontal sections of the root apical periodontal ligament (PDL) and alveolar bone crest (ABC) regions. **(b)** Representative immunofluorescence staining of Bmp7 in corresponding frontal sections. Red arrows indicate distinct expression patterns of Bmp2 and Bmp7 within the PDL space. Scale bar = 100 µm.

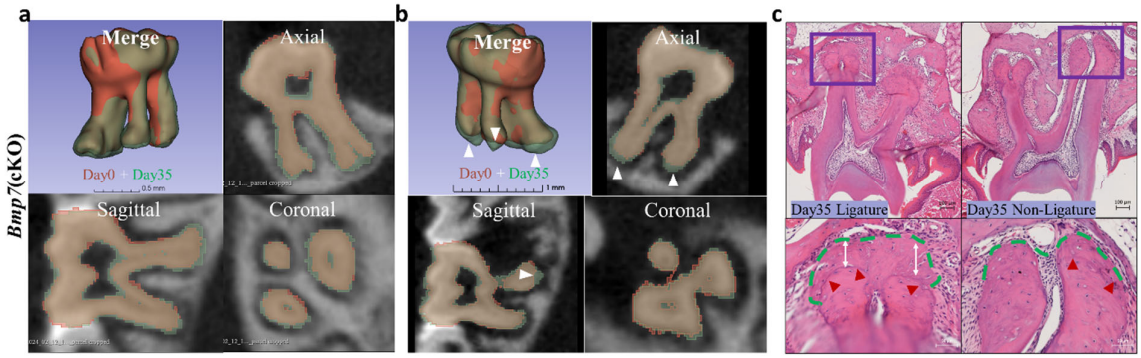

Supplementary Figure 6. Root cementum deposition in Bmp7 conditional knockout mice (cKO).

(a) Overlaid micro–computed tomography (micro-CT) images of second molars on the non-ligature side at Day 0 (red) and Day 35 (green) demonstrating a relatively little cementum deposition at the root apex in Bmp7 cKO mice. **(b)** Overlaid micro-CT images of second molars on the ligature side at Day 0 (red) and Day 35 (green) showing cementum deposition in Bmp7 conditional knockout (cKO) mice compared with the pre-injury state (white arrows). **(c)** Representative H/E-stained sections showing cementum formation at the root apex; red arrowheads indicate a distinct dark staining line separating newly formed cementum from pre-existing cementum.

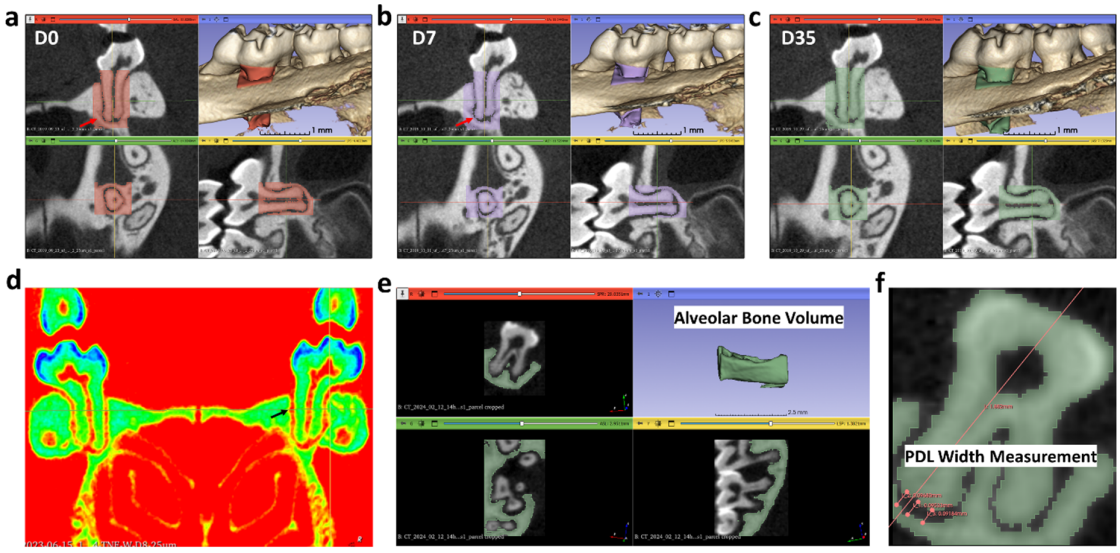

Supplementary Figure 7. Segmentation and Periodontal Ligament Width Measurement Using 3D Slicer

(a-c) The non-ligature-associated alveolar bone and palatal root of the first molar was cropped from the skull and isolated by segmentation. Tooth structures were included for quantitative analysis of mineralized tissue volume. **(d)** Representative 2D µCT axial view of the palatal root of the first molar comparing ligature and non-ligature sides. The black arrow indicates an irregular alveolar bone surface on the ligature-associated side. **(e)** Ligature-associated alveolar bone was cropped from the skull and isolated by segmentation. Tooth structures were manually erased prior to quantitative analysis of alveolar bone volume. **(f)** Periodontal ligament (PDL) width was measured using the Linear measurement tool in 3D Slicer. Measurements were taken along the tooth root axis as the distance between the cementum boundary and the inner surface of the alveolar bone.